CrystEngComm

PAPER

View Article Online
View Journal | View Issue

Cite this: *CrystEngComm*, 2014, **16**, 2230

A series of organic–inorganic hybrids based on lanthanide-substituted Dawson-type phosphotungstate dimers and copper–en linkers†

Hai-Yan Zhao,[a] Jun-Wei Zhao,*[b] Bai-Feng Yang,[a] Huan He[a] and Guo-Yu Yang*[ac]

Received 8th October 2013,
Accepted 2nd December 2013

DOI: 10.1039/c3ce42029a

www.rsc.org/crystengcomm

A family of organic–inorganic hybrid monolacunary Dawson phosphotungstate-based TM–Ln heterometallic derivatives $Na_2H(H_2en)_6[Cu(en)_2][Ln^{III}(\alpha_2\text{-}P_2W_{17}O_{61})_2]\cdot m\text{en}\cdot n H_2O$ (Ln = Tb^{III}, m = 2, n = 26 for **1**; Ln = Eu^{III}, m = 2, n = 28 for **2**; Ln = Sm^{III}, m = 4, n = 24 for **3**; Ln = Ce^{III}, m = 1, n = 21 for **4**) (Ln = lanthanide, TM = transition metal, en = 1,2-ethylenediamine) have been hydrothermally synthesized and structurally characterized by elemental analysis, powder X-ray diffraction (PXRD), IR spectra, thermo-gravimetric (TG) analyses and single-crystal X-ray diffraction. Notably, **1–4** are isomorphic and represent the first family of 1-D chain-like architectures constructed by 1:2-type mono-Ln substituted Dawson-type $[Ln^{III}(\alpha_2\text{-}P_2W_{17}O_{61})]_2^{17-}$ dimeric units and $[Cu(en)_2]^{2+}$ connectors, in which the sandwich-type Ln-substituted monolacunary Dawson phosphotungstate fragment is found for the first time in TM–Ln–polyoxotungstate chemistry. Furthermore, the variable-temperature magnetic susceptibility of **1** has been investigated.

Introduction

Nowadays, the design and synthesis of organic–inorganic hybrids has become a significant research area as they combine functional organic components and inorganic building blocks into unique materials through various chemical or physical interactions.[1] Polyoxometalates (POMs), as anionic early transition metal oxide clusters,[2] are attractive inorganic building blocks for the construction of various inorganic–organic hybrid compounds, as they can not only provide a large number of terminal and bridging oxygen atoms as multidentate O-donor ligands that can capture TM or Ln cations, leading to new materials with diverse nuclearities and structural features, but also exhibit interesting catalytic, electrochemical, magnetic and photochemical properties.[3] Within this field, phosphotungstates are the largest POM subclass and probably the two most studied polyoxotungstate (POT) types are the famous plenary Keggin and Wells-Dawson families, which can be represented by $[PW_{12}O_{40}]^{3-}$ and $[P_2W_{18}O_{62}]^{6-}$.[4] Furthermore, their lacunary derivatives with diverse structural types can be easily obtained in one- or two-step processes in high yields and are often used as reactant precursors, such as monovacant $[PW_{11}O_{39}]^{7-}$ and $[P_2W_{17}O_{61}]^{10-}$,[5] trivacant $[PW_9O_{34}]^{9-}$ and $[P_2W_{15}O_{56}]^{12-}$ as well as hexa-vacant $[H_2P_2W_{12}O_{48}]^{12-}$,[6] which provide us with abundant initial materials to search for and exploit their derivatives. One of the most current interests in this area is to embellish lacunary POT building blocks with Ln/TM cations in the presence of organic ligands to obtain functionalized organic–inorganic hybrid POM materials.[7] In the past several decades, although a rapidly growing class of TM/Ln/TM–Ln containing Keggin-type POTs with a huge diversity of structures and realized applications have been extensively reported,[8] systematic investigations on inorganic–organic composite vacant Dawson-based TM/Ln/TM–Ln–POT derivatives are less developed, which may due to the fact that Dawson-type precursors are relatively unstable and highly reactive in solution.[9] For TM-containing Dawson-type POTs, the use of lacunary Dawson POTs as inorganic multidentate building blocks to incorporate a large number of paramagnetic TM clusters, producing large numbers of TM-substituted Dawson POTs with interesting properties.[8e,9b,10] For Ln-containing Dawson-type POTs, although the coordinative flexibility and exceptional optical and magnetic properties arising from the 4f electrons of Ln cations render them promising linkers of lacunary Dawson POT fragments, lacunary Dawson-type POTs concatenated by Ln cations are comparatively rare,[10d,11] which may be caused by low stability constants for the binding of Ln cations with Dawson-type

[a] *DOE Key Laboratory of Cluster Science, School of Chemistry, Beijing Institute of Technology, Beijing 100081, China. E-mail: ygy@bit.edu.cn; Fax: +86 10 6891 8572*
[b] *Henan Key Laboratory of Polyoxometalate Chemistry, College of Chemistry and Chemical Engineering, Henan University, Henan 475004, Kaifeng, China. E-mail: zhaojunwei@henu.edu.cn*
[c] *State Key Laboratory of Structural Chemistry, Fujian Institute of Research on the Structure of Matter, Chinese Academy of Sciences, Fujian 350002, Fuzhou, China. E-mail: ygy@fjirsm.ac.cn; Fax: +86 591 8371 0051*

† Electronic supplementary information (ESI) available: XRD, IR, additional figures and tables. CCDC 930582–930585. For ESI and crystallographic data in CIF or other electronic format see DOI: 10.1039/c3ce42029a

POTs.[11c] Compared with the above mentioned limited Dawson-based TM/Ln-substituted POTs reported up to now, the chemistry of TM–Ln heterometal Dawson-type POT derivatives is still in its infancy and extraordinarily underexplored.[12] This problem can be attributed, as least partially, to the fact that POM clusters usually have large negative charges and oxygen rich compositions. Hence, their reaction with the highly oxophilic Ln elements results in precipitation instead of a crystalline form in most cases. Furthermore, the reactive activity between the polyoxoanions (POAs) and TM ions is relatively weak. So reaction competition unavoidably exists among the highly negative POAs, strongly oxyphilic Ln cations, and relatively less active TM cations in aqueous solution systems, which impedes single-crystal X-ray diffraction studies.[13] Hitherto, only a few examples of TM–Ln heterometallic Dawson-type POTs have been communicated as follows: in 2008, Kögerler and co-workers discovered two novel Dawson-type phosphotungstate-based Ce^{IV}–Mn^{IV} heterometallic clusters $[\{\alpha\text{-}P_2W_{15}O_{56}\}_6\{Ce_3Mn_2(\mu_3\text{-}O)_4(\mu_2\text{-}OH)_2\}_3(\mu_2\text{-}OH)_2(H_2O)_2(PO_4)]^{47-}$ (ref. 12*a*) and $[\{\alpha\text{-}P_2W_{16}O_{57}(OH)_2\}\{CeMn_6O_9(O_2CCH_3)_8\}]^{8-}$.[12b] In 2009, Wang's group reported two $\{P_2W_{12}\}$-based $[K_3\subset\{GdMn(H_2O)_{10}\}\{HMnGd_2(Tart)O_2(H_2O)_{15}\}\{P_6W_{42}O_{151}(H_2O)_7\}]^{11-}$ (Tart = tartaric acid anion) and $[K_3\subset\{GdCo(H_2O)_{11}\}_2\{P_6W_{41}O_{148}(H_2O)_7\}]^{13-}$ (ref. 12*c*) as well as one triple-Dawson-type $\{[Ce_3\ Mn_2O_6(OAc)_6(H_2O)_9]_2[Mn_2P_2W_{16}O_{60}]_3\}^{20-}$.[12d] In 2012, Kortz's group made the horseshoe-shaped 16-iron(III)-containing POT $[Fe_{16}O_2(OH)_{23}(H_2O)_9P_8W_{49}O_{189}Ln_4(H_2O)_{19}]^{11-}$ (Ln = Eu,Gd);[12e] Lately, Ma's group isolated a unique $\{P_2W_{15}\}$-based self-penetrating heterometallic POT $\{[Ce_4(H_2O)_{22}(dpdo)_5][Mn_2HP_2W_{15}O_{56})_2\}^{2-}$ (dpdo = 4,4′-bipyridine-*N*,*N*′-dioxide).[12f] From the above, it can be concluded that the reports on Dawson-type POTs containing TM–Ln heterometals are very limited and almost all of the afore-mentioned Dawson-type compounds are synthesized under conventional aqueous solution conditions.[12a–e] However, systems containing vacant Dawson-type phosphotungstates and TM as well as Ln cations in the participation of organic components under hydrothermal conditions remain unexplored, which provides us with a great opportunity and inspires our research interest.

As a continuation of the exploitation and synthesis of TM–Ln heterometallic Dawson-type POTs, we have investigated the reactions between $[H_2P_2W_{12}O_{48}]^{12-}$ POAs, Ln and TM cations in the presence of en and oxalic acid dehydrate in order to construct unexpected inorganic–organic hybrid compounds. Here, we report the hydrothermal syntheses, characterization and crystal structures of four unprecedented organic–inorganic hybrid TM–Ln heterometallic Dawson-type POTs $Na_2H(H_2en)_6[Cu(en)_2][Ln^{III}(\alpha_2\text{-}P_2W_{17}O_{61})_2]\cdot m\text{en}\cdot n H_2O$ (Ln = Tb^{III}, m = 2, n = 26 for **1**; Ln = Eu^{III}, m = 2, n = 28 for **2**; Ln = Sm^{III}, m = 4, n = 24 for **3**; Ln = Ce^{III}, m = 1, n = 21 for **4**). Notably, they represent the first family of 1-D 3d–4f Dawson-type POTs built by sandwich-type Ln-substituted mono-lacunary Dawson phosphotungstates and copper–en linkers, in which the dimeric mono-Ln substituted Dawson-type $[Ln(\alpha_2\text{-}P_2W_{17}O_{61})]_2^{17-}$ subunits are found for the first time in 3d–4f–POT chemistry.

Experimental

Materials and methods

The lacunary POM precursor $K_{12}[\alpha\text{-}H_2P_2W_{12}O_{48}]\cdot 24H_2O$ was prepared according to the literature and identified by IR spectra.[6c] All the other chemicals were obtained from commercial sources and used without further purification. Elemental analyses of C, H and N were carried out with a Vario EL III elemental analyzer. IR spectra (KBr pellets) were recorded on a Thermo Scientific Nicolet iS10 FT–IR Spectrometer over a range of 4000–400 cm^{-1}. PXRD patterns were obtained using a Bruker D8 ADVANCE XRD diffractometer with Cu Kα radiation (λ = 1.54056 Å). TG analyses were performed on a TGA Q50 thermal analyzer in a flowing air atmosphere with a heating rate of 10 °C min^{-1} from 30 to 850 °C. Variable temperature susceptibility measurements for **1** were carried out in the temperature range of 2–300 K at a magnetic field of 1 kOe on a polycrystalline sample with a Quantum Design MPMS XL-5 SQUID magnetometer. All the magnetic susceptibility data were corrected for magnetization of the sample holder and for diamagnetic contribution estimated from Pascal's constants.

Synthesis of $Na_2H(H_2en)_6[Cu(en)_2][Tb^{III}(\alpha_2\text{-}P_2W_{17}O_{61})_2]\cdot 2en\cdot 26H_2O$ (1)

A mixture of $K_{12}[\alpha\text{-}H_2P_2W_{12}O_{48}]\cdot 24H_2O$ (0.280 g), $Cu(Ac)_2\cdot H_2O$ (0.118 g), oxalic acid dehydrate (0.213 g) and $Tb(Ac)_3\cdot 6H_2O$ (0.105 g) were stirred in distilled water (10 mL), then en (0.15 mL) was added under stirring. Finally, an aqueous solution (1 mL) of 1 M NaCl was added dropwise with continuous stirring for 20 min (pH_i = 5.1). The resulting solution was transferred into a 30 mL Teflon-lined autoclave, heated under autogenous pressure at 80 °C for 5 days, and then cooled to room temperature naturally in air (pH_f = 5.6). Gray plate crystals were obtained by filtration, washed with distilled water and dried in air. Yield: 35% based on $K_{12}[\alpha\text{-}H_2P_2W_{12}O_{48}]\cdot 24H_2O$. Anal. calcd for **1**, $C_{20}H_{145}N_{20}O_{148}Na_2CuTbP_4W_{34}$: C 2.48, H 1.51, N 2.89; found: C 2.61, H 1.73, N 2.75. IR bands (cm^{-1}) for **1**: 3439s, 3298w, 3240w, 3143m, 3029w, 2927w, 1617s, 1512s, 1453w, 1384s, 1325w, 1084s, 1054s, 1027w, 940s, 877m, 823m, 776s, 723m, 522s.

Synthesis of $Na_2H(H_2en)_6[Cu(en)_2][Eu^{III}(\alpha_2\text{-}P_2W_{17}O_{61})_2]\cdot 2en\cdot 28H_2O$ (2)

The preparation of **2** is similar to **1**, except that $Eu(Ac)_3\cdot 6H_2O$ (0.094 g) replaced $Tb(Ac)_3\cdot 6H_2O$ (pH_i = 4.9). Gray plate crystals were obtained by filtration, washed with distilled water and dried in air (pH_f = 5.3). Yield: 27% based on $K_{12}[\alpha\text{-}H_2P_2W_{12}O_{48}]\cdot 24H_2O$. Anal. calcd for **2**, $C_{20}H_{149}N_{20}O_{150}Na_2CuEuP_4W_{34}$: C 2.47, H 1.55, N 2.88; found: C 2.60, H 1.79, N 2.76. IR bands (cm^{-1}) for **2**: 3442s, 3295w, 3244w, 3144w, 2859w, 2924s, 2853w, 1610s, 1512m, 1460w, 1424w, 1384s, 1085s, 1054s, 1024w, 940s, 877m, 819m, 775s, 723m, 522s.

Synthesis of $Na_2H(H_2en)_6[Cu(en)_2][Sm^{III}(\alpha_2\text{-}P_2W_{17}O_{61})_2]\cdot 4en\cdot 24H_2O$ (3)

The preparation of **3** is similar to **1**, except that $Sm(Ac)_3\cdot 6H_2O$ (0.098 g) replaced $Tb(Ac)_3\cdot 6H_2O$ (pH_i = 5.2). Gray plate crystals were obtained by filtration, washed with distilled water and dried in air (pH_f = 5.7). Yield: 21% based on $K_{12}[\alpha\text{-}H_2P_2W_{12}O_{48}]\cdot 24\ H_2O$. Anal. calcd for **3**, $C_{24}H_{157}N_{24}O_{146}Na_2CuSmP_4W_{34}$: C 2.95, H 1.62, N 3.44; found: C 3.09, H 1.88, N 3.32. IR bands (cm^{-1}) for **3**: 3439s, 3298w, 3253w, 2962w, 2924m, 2853w, 1631s, 1511 m, 1384s, 1085s, 1056m, 1027w, 940s, 880m, 819m, 778s, 723m, 525s.

Synthesis of $Na_2H(H_2en)_6[Cu(en)_2][Ce^{III}(\alpha_2\text{-}P_2W_{17}O_{61})_2]\cdot en\cdot 21\ H_2O$ (4)

The preparation of **4** is similar to **1**, except that $(NH_4)_2SO_4\cdot Ce(SO_4)_2\cdot 4H_2O$ (0.117 g) replaced $Tb(Ac)_3\cdot 6H_2O$ (pH_i = 5.3). Gray plate crystals were obtained by filtration, washed with distilled water and dried in air (pH_f = 5.6). Yield: 16% based on $K_{12}[\alpha\text{-}H_2P_2W_{12}O_{48}]\cdot 24H_2O$. Anal. calcd for **4**, $C_{16}H_{117}N_{16}O_{142}Na_2CuCeP_4W_{34}$: C 2.27, H 1.34, N 2.65; found: C 1.92, H 1.43, N 2.42. IR bands (cm^{-1}) for **4**: 3440s, 3247w, 3148w, 2962w, 2924m, 2856w, 1611s, 1500m, 1384s, 1121w, 1085s, 942s, 909w, 806m, 777s, 729m, 522s.

X-Ray crystallography

The intensity data of **1–4** were collected on a Gemini A Ultra diffractometer with graphite-monochromated Mo Kα (λ = 0.71073 Å) at 293(2) K. The SADABS program was used for the absorption correction.[14] The structures were solved by the direct method and refined on F^2 by full-matrix least-squares methods using the SHELX 97 program package.[15] No hydrogen atoms associated with the water molecules were located from the difference Fourier map. The positions of the hydrogen atoms attached to the carbon and nitrogen atoms were geometrically placed. All hydrogen atoms were refined isotropically as a riding mode using the default SHELXTL parameters. All non-hydrogen atoms were refined anisotropically except for partial oxygen atoms, carbon atoms, nitrogen atoms and water molecules (the details are seen in the ESI†).

Additionally, because the structures of **1–4** are larger than those of simple coordination complexes and there is a large amount of heavy atoms in the structures, it is very difficult to refine these large structures. Moreover, the quality of crystals is not very good and the absorption coefficient is large, which usually leads to cases where the quality of the intensity data is not perfect. As a result, in all of the structures there is a discrepancy between the formulas determined by elemental analyses and those deduced from the crystallographic atom list. In the refinements for **1–4**, only partial lattice water molecules and free en molecules can be accurately assigned from the Fourier maps. However, it is clear that there are still very large accessible solvent voids (from the checkcif reports), which can incorporate potential molecules in the crystal structures, indicating that some more counter cations and water molecules should exist in the structures, but cannot be found from the weak residual electron peaks. Based on the charge-balance considerations, elemental analyses and TG analyses, the rest have been directly included in the final molecular formula, which is a common phenomenon encountered in POM chemistry.[16] A summary of the crystal data and structure refinements for **1–4** are listed in Table 1. CCDC reference no. 930582–930585 for **1–4**.

Table 1 Crystal data and structure refinement details for **1–4**

Compound	1	2	3	4
Empirical formula	$C_{20}H_{145}N_{20}O_{148}Na_2CuTbP_4W_{34}$	$C_{20}H_{149}N_{20}O_{150}Na_2CuEuP_4W_{34}$	$C_{24}H_{157}N_{24}O_{146}Na_2CuSmP_4W_{34}$	$C_{18}H_{127}N_{18}O_{143}Na_2CuCeP_4W_{34}$
Formula weight	9677.78	9706.85	9753.39	9508.80
Crystal system	Monoclinic	Monoclinic	Monoclinic	Monoclinic
Space group	*C*2/*c*	*C*2/*c*	*C*2/*c*	*C*2/*c*
a (Å)	48.2903(15)	48.3988(17)	48.4356(12)	48.5506(11)
b (Å)	13.6014(3)	13.6295(4)	13.5979(3)	13.6364(5)
c (Å)	22.1554(5)	22.1644(6)	22.1157(5)	22.1072(5)
β (°)	100.647(3)	100.660(3)	100.540(2)	100.436(2)
Volume (Å^3)	14 301.5(6)	14 368.5(8)	14 320.1(6)	14 394.1(7)
Z	4	4	4	4
ρ_{calcd} (g cm^{-3})	4.495	4.487	4.524	4.388
μ (mm^{-1})	28.036	27.851	27.917	27.674
F (000)	17 124	17 196	17 304	16 760
Crystal size (mm^3)	0.31 × 0.15 × 0.10	0.25 × 0.10 × 0.08	0.29 × 0.12 × 0.07	0.30 × 0.11 × 0.06
θ range (°)	2.88–25.20	2.88–25.20	2.76–25.20	2.97–25.00
Limiting indices	$-57 \le h \le 57$ $-16 \le k \le 16$ $-26 \le l \le 26$	$-57 \le h \le 52$ $-15 \le k \le 16$ $-26 \le l \le 26$	$-58 \le h \le 58$ $-15 \le k \le 16$ $-22 \le l \le 26$	$-57 \le h \le 56$ $-13 \le k \le 16$ $-22 \le l \le 26$
Reflections collected/unique	61 600/12 847	37 770/12 910	65 286/12 876	34 965/12 489
Data/restraints/parameters	12 847/43/916	12 910/19/952	12 876/89/961	12 489/90/903
GOF[a] on F^2	1.043	1.075	1.056	1.012
R_1/wR_2[b] [$I > 2\sigma(I)$]	0.0470/0.1190	0.0367/0.0795	0.0424/0.1034	0.0746/0.1820
R_1/wR_2[b] (all data)	0.0581/0.1234	0.0545/0.0848	0.0601/0.1127	0.0934/0.1974

[a] GOF = $[\sum w(F_o^2 - F_c^2)^2/(n_{obc} - n_{param})]^{1/2}$. [b] $R_1 = ||F_o| - |F_c||/\sum|F_o|$, $wR_2 = [\sum w(F_o^2 - F_c^2)^2/\sum w(F_o^2)^2]^{1/2}$.

Results and discussion

Synthesis

As is known, in the reaction of a TM–Ln–POT system, oxyphilic Ln cations are easily combined with the surfaces of lacunary POAs, usually leading to precipitation rather than crystallization, while the reactions between POAs and TM ions are less active. As a result, when Ln and TM ions simultaneously react with POAs, reaction competition will unavoidably exist among the strongly oxyphilic Ln cations and the relatively less active TM ions in such a mixed reaction system.[13a] Moreover, it can be found that TM–Ln heterometallic Dawson-type POTs are very limited up to now (Table 2),[12] so it is still a current challenge to explore suitable synthetic conditions to obtain new charming Dawson-type POT-based TM–Ln heterometallic aggregates. In general, there are two synthetic strategies to approach TM–Ln heterometallic POTs, namely, s one-pot procedure method and a step-by-step assembly method. The one-pot procedure is the *in situ* reaction of simple starting materials (d and f cations, POMs and organic ligands). In contrast, the step-by-step assembly contains two routes: (i) reactions of TM–Ln heterometal precursors with other synthons, (ii) reactions of preformed TM- or Ln-substituted clusters with other synthons.[12f] Since the pioneering work by Fang and Kögerler, only three examples of Dawson-POT-based TM–Ln heterometal compounds have been isolated using the step-by-step assembly method.[12a,b,f] Simultaneously, it is well-known that the conventional solution method is not suitable for preparing organic–inorganic hybrid TM–Ln POTs, which usually require all the starting chemicals to be able to dissolve together to form a solution without any precipitate at ambient pressure. In contrast, the high pressure and temperature of hydrothermal reactions can cause a reaction to shift from the kinetic to the thermodynamic domain and overcome the difficulties due to differential solubilities of organic and inorganic starting materials.[7a] Therefore, currently, one effective approach is the incorporation of TM and Ln cations into lacunary POT matrixes under hydrothermal environments to construct POT-based Ln–TM heterometallic derivatives with diverse structural features and interesting properties. Nevertheless, as reported in previous literature, almost all of the TM–Ln heterometallic Dawson-type POTs are obtained by a conventional solution method except $Na_2[Ce_4(H_2O)_{22}(dpdo)_5](Mn_2HP_2W_{15}O_{56})_2{\cdot}8H_2O$, hydrothermally synthesized by preconstructed tetra-Mn^{II}-substituted sandwich-type cluster precursors (Table 2).[12f] To date, the more facile and convenient one-pot hydrothermal method has not been used for the synthesis of Dawson-POT-based TM–Ln heterometallic compounds, providing us with great interest and opportunity.

Furthermore, the multivacant Dawson-type POA $K_{12}[\alpha\text{-}H_2P_2W_{12}O_{48}]{\cdot}24H_2O$ is used as a starting material instead of the $K_{10}[\alpha_2\text{-}P_2W_{17}O_{61}]{\cdot}20H_2O$ precursor since the multivacant Dawson-type POA contains more vacant sites that can "capture" more TM or Ln ions and connect them together into huge clusters. Furthermore, the metastable $[\alpha\text{-}H_2P_2W_{12}O_{48}]^{12-}$ POA is an ideal precursor because this POM is easy to isomerize or partly decompose in solution and can be transformed into other vacant building blocks, which provides a large amount of possibilities for the isolation of diverse fascinating Dawson-type POT-based aggregates.[12d]

On the basis of the aforementioned considerations, **1–4** were successfully accomplished by the one-pot reaction of the hexavacant polyoxotungstate precursor $[H_2P_2W_{12}O_{48}]^{12-}$ with TM and Ln cations assisted with organic molecules (en and oxalic acid dehydrate) under hydrothermal conditions. Although the $[\alpha\text{-}H_2P_2W_{12}O_{48}]^{12-}$ starting material was employed to prepare **1–4**, all the products include $[\alpha_2\text{-}P_2W_{17}O_{61}]^{10-}$ fragments. However, when $K_{10}[\alpha_2\text{-}P_2W_{17}O_{61}]{\cdot}20H_2O$ or $Na_{12}[P_2W_{15}O_{56}]{\cdot}18H_2O$ replaced $K_{12}[\alpha\text{-}H_2P_2W_{12}O_{48}]{\cdot}24H_2O$ under similar conditions, **1–4** could not be afforded, which suggests that the transformation of $[\alpha\text{-}H_2P_2W_{12}O_{48}]^{12-} \rightarrow [\alpha_2\text{-}P_2W_{17}O_{61}]^{10-}$ plays an important role in the formation of **1–4**. It is known that this species rearranges quickly in aqueous, acidic media to the monolacunary $[\alpha_1\text{-}P_2W_{17}O_{61}]^{10-}$, which in turn is unstable and rearranges to the more stable $[\alpha_2\text{-}P_2W_{17}O_{61}]^{10-}$.[6c] This transformation has already been observed in previous studies.[17] To investigate the effect of different TM ions on structural diversity, we also replace the Cu^{II} ion with Mn^{II}, Fe^{II}, Co^{II}, Ni^{II} or Zn^{II} cations, but after plenty of parallel experiments, we could not obtain the expected products but only amorphous precipitates, which is due to the fact that the flexible coordination modes and the Jahn–Teller effect of Cu^{II} cations can overcome steric hindrance to favourably form novel structures, suggesting that Cu^{2+} ions play a key factor in the construction of the products.

Additionally, en and oxalic acid dehydrate were simultaneously introduced to the reaction mixture of $[H_2P_2W_{12}O_{48}]^{12-}$, Cu^{2+} and Ln cations, resulting in four new Cu–Ln heterometallic Dawson phosphotungstates. Our original expectation was that oxalic acid can act as a bridging ligand to connect the TM/Ln centers. However, unexpectedly, only the en component is included in the products. Our comparison experiments prove that $H_2C_2O_4$ is necessary for the syntheses of **1–4** even though it is not incorporated in the final products. After plenty of parallel experiments, it was found that these compounds could not be obtained when $H_2C_2O_4$ is moved away from the starting materials, indicating the presence of $H_2C_2O_4$ is crucial for the preparation of **1–4**. Hence, it can be deduced that the presence of adapted exogenous multicarboxylic acid ligands might stabilize the Ln ions and/or reduce the reactivity of the Ln ions with POAs, which may have a synergistic action with other components in the system. Though the detailed mechanism is not well understood, similar phenomena have been observed under hydrothermal conditions in our previous studies.[11c,18] A profound investigation on this reaction mechanism is in progress. Moreover, we also attempted to further explore the effect of other organic ligands on the products by replacing ethylenediamine with 1,2-diaminopropane or replacing oxalic acid dehydrate with malonic/succinic acid under similar conditions. Unfortunately,

Table 2 Summary of the synthetic conditions and related phases in the preparation of TM–Ln heterometallic Dawson-type POTs

Major reactant	*T*/°C	Synthetic method	Reaction system	Products
$Na_{12}[P_2W_{15}O_{56}]\cdot 18H_2O/NaH_2PO_4/KCl/[Ce^{IV}{}_3Mn^{IV}{}_2O_6(O_2CMe)_{7.5}(NO_3)_3]\cdot(HO_2CMe)_{0.5}(H_2O)_2$	80	Solvent evaporation	H_2O	$K_{36}Na_{11}[\{\alpha\text{-}P_2W_{15}O_{56}\}_6\{Ce_3Mn_2(\mu_3\text{-}O)_4(\mu_2\text{-}OH)_2\}_3(\mu_2\text{-}OH)_2(H_2O)_2(PO_4)]\cdot 106H_2O$[12a]
$Na_{12}[P_2W_{15}O_{56}]\cdot 18H_2O/(CH_3)_2NH\cdot HCl/CeMn_6O_9(O_2CCH_3)_9(NO_3)(H_2O)_2$	70	Solvent evaporation	HOAc–H_2O	$[(CH_3)_2NH_2]_6H_2[\{\alpha\text{-}P_2W_{16}O_{57}(OH)_2\}\{CeMn_6O_9(O_2CCH_3)_8\}]\cdot 20H_2O$[12b]
$K_{12}[H_2P_2W_{12}O_{48}]\cdot 24H_2O/Gd(NO_3)_3/Na_2C_4H_4O_6\cdot 2H_2O/MnCl_2$	40	Solvent evaporation	H_2O	$K_3Na_8[K_3\subset\{GdMn(H_2O)_{10}\}\{HMnGd_2(Tart)O_2(H_2O)_{15}\}\{P_6W_{42}O_{151}(H_2O)_7\}]\cdot 44H_2O$[12c]
$K_{12}[H_2P_2W_{12}O_{48}]\cdot 24H_2O/CoCl_2/Gd(NO_3)_3/(CH_3)_2NH\cdot HCl$	Room temperature	Solvent evaporation	H_2O	$K_3Na_{10}[K_3\subset\{GdCo(H_2O)_{11}\}_2\{P_6W_{41}O_{148}(H_2O)_7\}]\cdot 43H_2O$[12c]
$K_{12}[H_2P_2W_{12}O_{48}]\cdot 24H_2O/(NH_4)_2[Ce(NO_3)_6]/Mn(OAc)_2\cdot 4H_2O$	Room temperature	Solvent evaporation	H_2O–HOAc HOAc–NaOAc	$Na_{20}\{[Ce_3Mn_2O_6(OAc)_6(H_2O)_9]_2[Mn_2P_2W_{16}O_{60}]_3\}\cdot 21H_2O$[12d]
$K_{28}Li_5[H_7P_8W_{48}O_{184}]\cdot 92H_2O/FeCl_3\cdot 6H_2O/EuCl_3\cdot 6H_2O/30\%\ H_2O_2/NaCl/$	80	Solvent evaporation	LiOAc–HOAc	$K_{8.5}Na_{0.5}Li_{0.5}Eu_{0.5}[Fe_{16}O_2(OH)_{23}(H_2O)_9P_8W_{49}O_{189}Eu_4(H_2O)_{19}]\cdot 70H_2O$[12e]
$K_{28}Li_5[H_7P_8W_{48}O_{184}]\cdot 92H_2O/FeCl_3\cdot 6H_2O/GdCl_3\cdot 6H_2O/30\%\ H_2O_2/NaCl$	80	Solvent evaporation	LiOAc–HOAc	$K_9LiNa[Fe_{16}O_2(OH)_{23}(H_2O)_9P_8W_{49}O_{189}Gd_4(H_2O)_{19}]\cdot 50H_2O$[12e]
$Na_{16}[Mn_4(H_2O)_2(P_2W_{15}O_{56})_2]\cdot 53H_2O/dpdo/Ce(NO_3)_3\cdot 6H_2O$	160	Hydrothermal technique	H_2O	$Na_2[Ce_4(H_2O)_{22}(dpdo)_5](Mn_2HP_2W_{15}O_{56})_2\cdot 8H_2O$[12f]
$K_{12}[\alpha\text{-}H_2P_2W_{12}O_{48}]\cdot 24H_2O/Ln(OAc)_3\cdot 6H_2O/en/NaCl/Cu(Ac)_2\cdot H_2O/H_2C_2O_4\cdot 2H_2O$	80	Hydrothermal technique	H_2O	**1–4** (Ln = Tb^{III}, Eu^{III}, Sm^{III}, Ce^{III})

no isostructural compound was obtained. It can be seen that the size and shape of the organic ligands can influence the formation of the resulting products.

Structure description

The experimental PXRD patterns of **1–4** are in good agreement with the simulated PXRD patterns from the single-crystal X-ray diffraction, demonstrating the good phase purity of the samples (Fig. S1, ESI†). The difference in intensity between them may be due to the variation in the preferred orientation of the powder sample during the collection of the experimental PXRD pattern. In addition, the bond–valence sum calculations[19] indicate that the oxidation states of the W, Ln and Cu elements in these compounds are +6, +3 and +2, respectively.

X-ray single-crystal structural analyses show that **1–4** crystallize in the monoclinic space group *C*2/*c* and are isomorphic only with slight differences in bond lengths, bond angles and the number of lattice waters. Thus, only **1** is described in detail as an example below. The skeleton of **1** consists of a dimeric $[Tb^{III}(\alpha_2\text{-}P_2W_{17}O_{61})_2]^{17-}$ POA, six diprotonated $[H_2en]^{2+}$ ions, one bridging $[Cu(en)_2]^{2+}$ cation, two Na^+ ions, two free en molecules, one proton as well as twenty six lattice water molecules. The sandwich 1:2-type $[Tb(\alpha_2\text{-}P_2W_{17}O_{61})_2]^{17-}$ subunit is formed by the incorporation of the $Tb1^{III}$ cation into the classical plenary Dawson-type $[\alpha\text{-}P_2W_{18}O_{62}]^{6-}$ POA by removal of a polar W=O_d group (Fig. 1). The $Tb1^{III}$ cation exhibits a distorted square antiprism geometry. Each eight-coordinated terbium center is sandwiched by two monovacant $[\alpha\text{-}P_2W_{17}O_{61}]^{10-}$ units, bonding to four available O atoms of the lacunary sites of the $[\alpha\text{-}P_2W_{17}O_{61}]^{10-}$ units with $Tb1^{III}$–O bond lengths ranging from 2.383(7) to 2.398(1) Å (Fig. 2a). Two $[\alpha\text{-}P_2W_{17}O_{61}]^{10-}$ "lobes" are disposed in a *syn* fashion. In addition, the $[Cu1(en)_2]^{2+}$ ion exhibits octahedral geometry with two N atoms from the chelating en ligands building the basal plane [Cu–N: 1.984(1)–2.009(1) Å] and two terminal oxygen atoms from two adjacent $[Tb(\alpha\text{-}P_2W_{17}O_{61})_2]^{17-}$ anions occupying the axial positions [Cu–O: 2.657(1) Å] (Fig. 2b). With such coordination geometries, each $[Tb(\alpha\text{-}P_2W_{17}O_{61})_2]^{17-}$ POA connects two $[Cu(en)_2]^{2+}$ bridges while each $[Cu(en)_2]^{2+}$ bridge links two $[Tb(\alpha\text{-}P_2W_{17}O_{61})_2]^{17-}$ subunits, resulting in an infinite 1-D chain running along the *c* axis (Fig. 2c). In addition, the

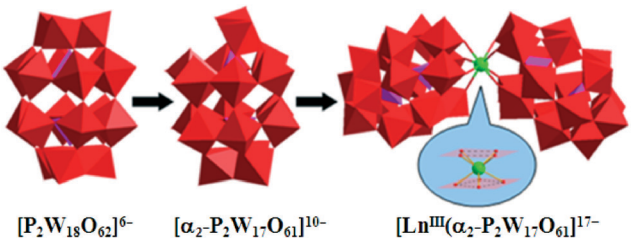

Fig. 1 The schematic process of Ln-substituted monovacant Dawson-type POT $[Ln^{III}(\alpha_2\text{-}P_2W_{17}O_{61})_2]^{17-}$ from the $[P_2W_{18}O_{62}]^{6-}$ POA in **1–4**; red $\{WO_6\}$ octahedra, purple $\{PO_4\}$ tetrahedra and green Ln cation.

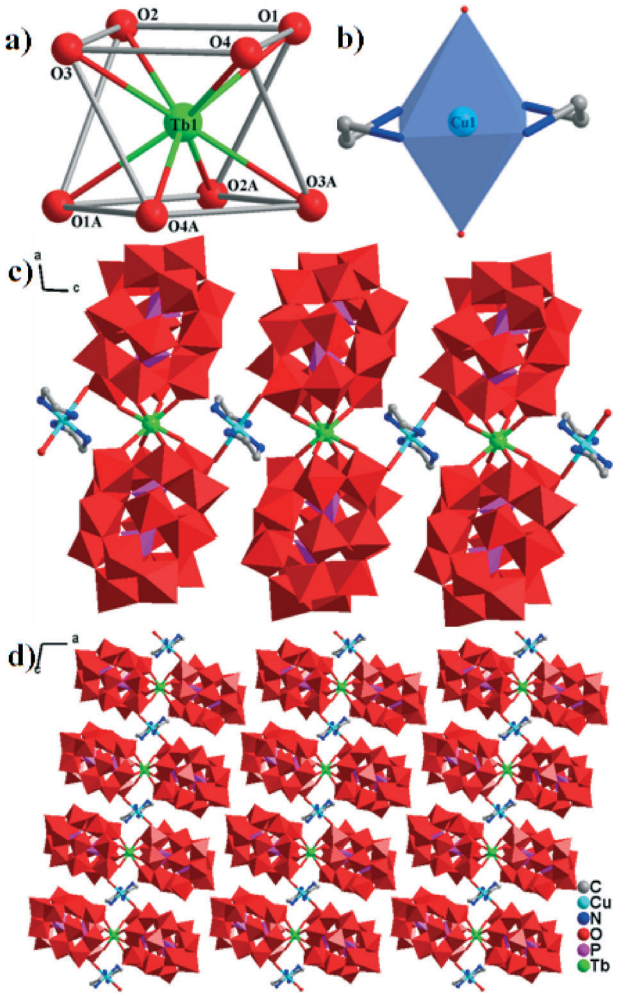

Fig. 2 (a) The coordination environment of the $Tb1^{III}$ cation in **1**; (b) the coordination environment of the $Cu1^{II}$ cation in **1**; (c) view of the 1-D chain of **1** along the *c* axis; (d) the packing arrangement of **1** in the *ac* plane. The atoms with the suffixes A are generated by the symmetry: A: –*x*, *y*, 1.5 – *z*.

1-D chains of **1** are packed in the –AAA– mode along the *b* axis (Fig. 2d). As far as we know, classical 1:2-type dimers made up of one Ln cation and two monovacant Keggin-type POM units have been widely investigated.[20] In addition, the 1:2 structural series made up of one Ln cation and two monovacant Dawson POM units has also been reported in Ln-POM chemistry,[11a,21] but the analogous 1:2-type $[Ln(\alpha_2\text{-}P_2W_{17}O_{61})_2]^{17-}$ dimers have never been reported in TM–Ln–POM chemistry so far.

1–4 all exhibit s 1-D chain-like architecture constructed by 1:2-type mono-Ln substituted Dawson-type $[Ln^{III}(\alpha_2\text{-}P_2W_{17}O_{61})]_2^{17-}$ dimers and $[Cu(en)_2]^{2+}$ connectors. By comparing the bond lengths of **1–4**, it can be clearly seen that the Ln–O bond lengths (Ce^{3+}, Sm^{3+}, Eu^{3+}, Tb^{3+}) decrease with increasing atomic number and decreasing ionic radii of the Ln^{3+} ions (Table 3), which is in accordance with the effect of the Ln contraction.[13a,20c] As far as we know, **1–4** represent the first family of 1-D organic–inorganic hybrid TM–Ln heterometallic derivatives containing both monolacunary Dawson phosphotungstate fragments and copper–en linkers.

Table 3 Comparison of the Ln–O bond lengths (Å) in **1**–**4**

Compounds	Selected Ln–O bond lengths				Average Ln–O bond lengths
1 (Tb)	2.383(1)	2.384(1)	2.392(1)	2.398(1)	2.389(1)
2 (Eu)	2.384(9)	2.404(9)	2.409(9)	2.410(9)	2.412(9)
3 (Sm)	2.408(8)	2.416(8)	2.421(8)	2.429(8)	2.419(8)
4 (Ce)	2.458(14)	2.464(16)	2.474(15)	2.475(13)	2.468(14)

More interestingly, the Ce^{III}–O bond lengths of the $[Ce(\alpha\text{-}P_2W_{17}O_{61})_2]^{17-}$ subunit in **4** are from 2.456(17) to 2.484(16) Å, which are significantly longer than those of Ce^{IV}-containing POMs and are consistent with other Ce^{III}-containing POMs.[22] It is worth noting that the Ce atom in **4** is in the +3 oxidation state (Table S1, ESI†), although the corresponding starting reagent is a cerium(IV) salt. Also, this is in agreement with the charge neutrality, coordination environments and bond lengths. The main reason must be that organoamines generally act not only as ligands but also as reducing agents under hydrothermal conditions. It is common that high oxidation state metals are reduced by organoamines under hydrothermal conditions.[23]

IR spectra

The IR spectra of **1**–**4** are very similar and exhibit characteristic peaks of the Dawson $\{P_2W_{17}O_{61}\}$ POAs in the low-wavenumber region (Fig. S2, ESI†).[22a] The bands at around 1085–1018 cm^{-1} can be assigned to the P–O stretching vibration. The W–O stretching vibration bands resulting from the Dawson-type structure, namely, ν(W–O_t), ν(W–O_b–W) and ν(W–O_c–W), appear at 942–940, 823–775, and 729–723 cm^{-1}, respectively (Table 4). On a close examination of the IR spectra for **1**–**4**, some of their stretching vibration bands split into two or three bands as a consequence of the lower symmetry of the POAs in **1**–**4** than those of the plenary Dawson clusters.[24] The similarity of their IR spectra in the low-wavenumber region may result from the presence of the monovacant Dawson-type fragments in their skeletons. However, in comparison with the IR spectrum of the hexavacant Dawson $K_{12}[\alpha\text{-}H_2P_2W_{12}O_{48}]\cdot 24H_2O$ precursor [911; 1128, 1080, 1013; 780 and 672 cm^{-1}, for ν(W–O_t); ν(P–O); ν(W–O_b–W) and ν(W–O_c–W)], the vibrational frequencies of ν(P–O) and ν(W–O_b–W) for **1**–**4** are red shifted, while those of ν(W–O_t) and ν(W–O_c–W) are blue shifted, which further confirms the structural transformation from $[\alpha\text{-}P_2W_{12}O_{48}]^{14-}$ to $[\alpha_2\text{-}P_2W_{17}O_{61}]^{10-}$ during the course of forming **1**–**4**. In addition, the bending vibration bands of the $-NH_2$ and $-CH_2$ groups appear at 1631–1500 and 1460–1384 cm^{-1} while the resonances appearing at 3298–3029 cm^{-1} and 2962–2853 cm^{-1} are attributable to the stretching vibrational bands of the $-NH_2$ and $-CH_2$ groups, respectively.[25] The occurrence of these resonance signals confirms the presence of en ligands in **1**–**4**. Apart from that, the vibration bands centered at 3442–3439 cm^{-1} are indicative of the presence of lattice water molecules. In short, the results of the IR spectra are consistent with the results obtained from the X-ray single-crystal structural analyses.

Table 4 Selected assignable IR data for the POAs of **1**–**4**

Compounds	Stretching frequency assignment/cm^{-1}			
	P–O	W–O_t	W–O_b–W	W–O_c–W
1	1084, 1054, 1027	940	823, 776	723
2	1085, 1054, 1024	940	819, 775	723
3	1085, 1056, 1027	940	819, 778	723
4	1085, 1059, 1018	942	806, 777	729

Thermal properties

To investigate the thermal stabilities of **1**–**4**, TG analyses were carried out in a flowing air atmosphere with a heating rate of 10 °C min^{-1} from 30 to 850 °C (Fig. S3, ESI†). The TG processes of **1**–**4** are very similar and reveal three steps of slow weight loss in the range of 30–850 °C.

For **1**, in the range of 30–248 °C, the first weight loss of 4.39% is caused by the loss of 26 lattice water molecules (calcd 4.84%). On further heating, the second weight loss of 7.37% between 248 and 624 °C is assigned to the decomposition of 10 en ligands and the dehydration of 13 protons (calcd. 7.42%). After 624 °C, a gradual weight loss of 2.55% until 850 °C is approximately attributable to the sublimation of 2 P_2O_5 molecules, derived from the combination of P and O atoms in the POAs (calcd 2.93%). In the case of **2**, the first weight loss of 5.12% between 30 and 170 °C is ascribed to the release of 28 lattice water molecules (calcd 5.19%). The second weight loss is 8.94% (calcd. 8.86%) from 170 °C to 670 °C, approximately assigned to the decomposition of 10 en ligands, the dehydration of 13 protons and the sublimation of 1 P_2O_5 molecule. The last weight loss of 1.60% between 670 and 850 °C corresponds to the sublimation of another P_2O_5 molecule (calcd 1.46%). With respect to **3**, the weight loss of 3.98% during the first step from 30 to 219 °C is assigned to the release of 24 lattice molecules (calcd 4.43%), followed by a weight loss of 6.69% from 219 to 585 °C, approximately corresponding to the loss of 12 en ligands, the dehydration of 13 protons and the sublimation of 1 P_2O_5 molecule (calcd 10.05%). After 585 °C, a gradual weight loss of 1.66% until 850 °C is approximately attributable to the sublimation of another P_2O_5 molecule (calcd 1.45%). For **4**, the first weight loss of 3.87% occurs in the range of 30–213 °C, corresponding well to the release of 21 lattice water molecules (calcd 3.98%). The second weight loss of 8.25% from 213 to 590 °C corresponds to the decomposition of 9 en ligands, the dehydration of 13 protons and the sublimation of 1 P_2O_5 molecule (calcd 8.41%). The third

weight loss of 1.28% between 590 and 850 °C corresponds to the sublimation of another P_2O_5 molecule (calcd 1.49%). In a word, all the observed experimental values are approximately consistent with the theoretical values.

Magnetic properties

It is well-known that heterometallic Cu–Ln compounds have attracted considerable attention owing to the presence of exchange interactions between spin carriers in the solid-state chemistry and materials.[26] The magnetic behavior of **1** is studied in the range of 2 to 300 K and the plots of χ_m, $\chi_m T$, χ_m^{-1} *versus* T are shown in Fig. 3. The value of χ_m slowly increases from 0.054 emu mol^{-1} at 300 K to 0.448 emu mol^{-1} at 40 K, then exponentially to the maximum of 4.280 emu mol^{-1} at 2 K. At 300 K, the $\chi_m T$ value is equal to 16.17 emu mol^{-1} K, which is slightly higher than the sum (12.20 emu mol^{-1} K)[27] of the contribution attributable to one isolated Tb^{III} cation in the $^7F_6$ group state (J = 6, g = 3/2) and one non-interacting Cu^{II} ion considering g = 2 per formula unit. Upon cooling, the $\chi_m T$ product gradually increases to a maximum of 17.96 emu mol^{-1} K at 48 K (Fig. 3a). This behavior of the $\chi_m T$ *versus* T plot may indicate that the S_{Tb} = 3 local spins tend to align somewhat along the same direction. The decrease in $\chi_m T$ on decreasing the temperature from 48 to 2 K can be ascribed to the thermal depopulation of the Stark sublevels of the Tb^{III} cations. Furthermore, as shown in Fig. 3b, the curve of χ_m^{-1} *versus* T between 70 K and 300 K follows the Curie–Weiss law with a Curie constant of C = 15.61 emu mol^{-1} K and a Weiss constant of θ = 9.71 K. However, as the temperature decreases from 70 K to 2 K, the relation of χ_m^{-1} *versus* T does not follow the Curie–Weiss law, which is related to the thermal depopulation of the Stark sublevels of the Tb^{III} cations.

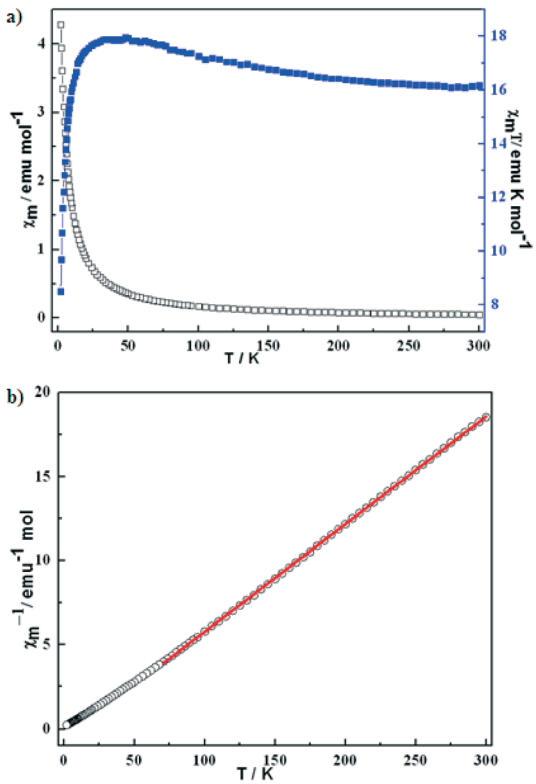

Fig. 3 (a) Temperature dependence of the $\chi_m T$ and χ_m values for **1** between 2 and 300 K; (b) temperature dependence of χ_m^{-1} for **1**. The red solid line is generated from the best-fit by the Curie–Weiss expression.

Conclusions

In conclusion, a class of unprecedented organic–inorganic hybrid Cu–Ln containing Dawson-type POTs have been successfully made using a one-pot hydrothermal method. Notably, they are isomorphic and represent the first family of 1-D chain-like TM–Ln containing Dawson-type POTs built by sandwich-type mono-Ln substituted Dawson $[Ln^{III}(\alpha_2\text{-}P_2W_{17}O_{61})]_2^{17-}$ dimers through $[Cu(en)_2]^{2+}$ linkers. As far as we know, the dimeric 1:2-type $[Ln(\alpha_2\text{-}P_2W_{17}O_{61})]_2^{17-}$ Dawson fragments are found for the first time in TM–Ln–POT chemistry. The successful preparation of **1–4** indicates that a one-pot hydrothermal self-assembly reaction of POMs, Ln salts, TM salts and organic ligands is an effective strategy in constructing organic–inorganic hybrid TM–Ln heterometallic POM hybrids. Further research will focus on making more novel heterometallic POTs by the judicious choice of different lacunary POT precursors and/or various organic ligands under hydrothermal conditions. More work in this field is currently ongoing in our group.

Acknowledgements

This work was supported by the NNSF of China (no. 91122028, 21221001, 50872133, 21101055), the NNSF for Distinguished Young Scholars of China (no. 20725101), and the 973 program (nos. 2014CB932101 and 2011CB932504).

Notes and references

1 (*a*) H. B. Yao, M. R. Gao and S. H. Yu, *Nanoscale*, 2010, **2**, 322; (*b*) R. Pardo, M. Zayat and D. Levy, *Chem. Soc. Rev.*, 2011, **40**, 672; (*c*) P. Innocenzi and B. Lebeau, *J. Mater. Chem.*, 2005, **15**, 3821; (*d*) M. S. Wang, G. Xu, Z. J. Zhang and G. C. Guo, *Chem. Commun.*, 2010, **46**, 361.

2 M. T. Pope and A. Müller, *Angew. Chem., Int. Ed. Engl.*, 1991, **30**, 34.

3 (*a*) A. Dolbecq, E. Dumas, C. R. Mayer and P. Mialane, *Chem. Rev.*, 2010, **110**, 6009; (*b*) U. Kortz, A. Müller, J. van Slageren, J. Schnack, N. S. Dalal and M. Dressel, *Coord. Chem. Rev.*, 2009, **253**, 2315; (*c*) J. M. Clemente-Juan, E. Coronado and A. Gaita-Ariño, *Chem. Soc. Rev.*, 2012, **41**, 7464; (*d*) C. Streb, *Dalton Trans.*, 2012, **41**, 1651; (*e*) D. E. Katsoulis, *Chem. Rev.*, 1998, **98**, 359; (*f*) L. Ni, J. Patscheider, K. K. Baldridge and G. R. Patzke, *Chem.–Eur. J.*, 2012, **18**, 13293.

4 C. L. Hill, *Chem. Rev.*, 1998, **98**, 1.

5 N. Haraguchi, Y. Okaue, T. Isobe and Y. Matsuda, *Inorg. Chem.*, 1994, **33**, 1015.

6 (*a*) A. P. Ginsberg, *Inorg. Synth.*, 1990, **27**, 100; (*b*) R. Massart, R. Contant, J. M. Fruchart, J. P. Ciabrini and M. Fournier,

Inorg. Chem., 1977, **16**, 2916; (*c*) R. Contant, *Inorg. Synth.*, 1990, **27**, 108.

7 (*a*) S. T. Zheng and G. Y. Yang, *Chem. Soc. Rev.*, 2012, **41**, 7623; (*b*) B. S. Bassil and U. Kortz, *Z. Anorg. Allg. Chem.*, 2010, **636**, 2222.

8 (*a*) R. S. Winter, J. Yan, C. Busche, J. S. Mathieson, A. Prescimone, E. K. Brechin, D. L. Long and L. Cronin, *Chem.–Eur. J.*, 2013, **19**, 2976; (*b*) L. Huang, J. Zhang, L. Cheng and G.-Y. Yang, *Chem. Commun.*, 2012, **48**, 9658; (*c*) F. Y. Li, W. H. Guo, L. Xu, L. F. Ma and Y. C. Wang, *Dalton Trans.*, 2012, **41**, 9220; (*d*) S. W. Zhang, Y. Wang, J. W. Zhao, P. T. Ma, J. P. Wang and J. Y. Niu, *Dalton Trans.*, 2012, **41**, 3764; (*e*) X. K. Fang, K. McCallum, H. D. Pratt III, T. M. Anderson, K. Dennis and M. Luban, *Dalton Trans.*, 2012, **41**, 9867; (*f*) H. H. Wu, S. Yao, Z. M. Zhang, Y. G. Li, Y. Song, Z. J. Liu, X. B. Han and E. B. Wang, *Dalton Trans.*, 2013, **42**, 342; (*g*) O. Oms, A. Dolbecq and P. Mialane, *Chem. Soc. Rev.*, 2012, **41**, 7497.

9 (*a*) L. Huang, L. Cheng, S. S. Wang, W. H. Fang and G. Y. Yang, *Eur. J. Inorg. Chem.*, 2013, **2013**, 1639; (*b*) S. S. Mal, B. S. Bassil, M. Ibrahim, S. Nellutla, J. van Tol, N. S. Dalal, J. A. Fernández, X. López, J. M. Poblet, R. N. Biboum, B. Keita and U. Kortz, *Inorg. Chem.*, 2009, **48**, 11636.

10 (*a*) Z. M. Zhang, S. Yao, Y. G. Li, Y. H. Wang, Y. F. Qi and E. B. Wang, *Chem. Commun.*, 2008, 1650; (*b*) S. G. Mitchell, C. Streb, H. N. Miras, T. Boyd, D. L. Long and L. Cronin, *Nature*, 2010, **2**, 308; (*c*) S. G. Mitchell, T. Boyd, H. N. Miras, D. L. Long and L. Cronin, *Inorg. Chem.*, 2010, **50**, 136; (*d*) L. Huang, L. Cheng, W. H. Fang, S. S. Wang and G. Y. Yang, *Eur. J. Inorg. Chem.*, 2012, **2013**, 1693; (*e*) C. Lydon, M. M. Sabi, M. D. Symes, D. L. Long, M. Murrie, S. Yoshii, H. Nojiri and L. Cronin, *Chem. Commun.*, 2012, **48**, 9819.

11 (*a*) Q. H. Luo, R. C. Howell, M. Dankova, J. Bartis, C. W. Williams, W. D. Horrocks, V. G. Young, A. L. Rheingold, L. C. Francesconi and M. R. Antonio, *Inorg. Chem.*, 2001, **40**, 1894; (*b*) Y. Lu, Y. Xu, Y. G. Li, E. B. Wang, X. X. Xu and Y. Ma, *Inorg. Chem.*, 2006, **45**, 2055; (*c*) S. W. Zhang, D. D. Zhang, P. T. Ma, Y. F. Liang, J. P. Wang and J. Y. Niu, *CrystEngComm*, 2013, **15**, 2992; (*d*) M. Zimmermann, N. Belai, R. J. Butcher, M. T. Pope, E. V. Chubarova, M. H. Dickman and U. Kortz, *Inorg. Chem.*, 2007, **46**, 1737.

12 (*a*) X. K. Fang and P. Kögerler, *Angew. Chem., Int. Ed.*, 2008, **47**, 8123; (*b*) X. K. Fang and P. Kogerler, *Chem. Commun.*, 2008, 3396; (*c*) S. Yao, Z. M. Zhang, Y. G. Li, Y. Lu, E. B. Wang and Z. M. Su, *Cryst. Growth Des.*, 2009, **10**, 135; (*d*) Y. W. Li, Y. G. Li, Y. H. Wang, X. J. Feng, Y. Lu and E. B. Wang, *Inorg. Chem.*, 2009, **48**, 6452; (*e*) A. H. Ismail, B. S. Bassil, G. H. Yassin, B. Keita and U. Kortz, *Chem.–Eur. J.*, 2012, **18**, 6163; (*f*) T. T. Yu, H. Y. Ma, C. J. Zhang, H. J. Pang, S. B. Li and H. Liu, *Dalton Trans.*, 2013, **42**, 16328.

13 (*a*) S. W. Zhang, J. W. Zhao, P. T. Ma, H. N. Chen, J. Y. Niu and J. P. Wang, *Cryst. Growth Des.*, 2012, **12**, 1263; (*b*) J. Y. Niu, S. W. Zhang, H. N. Chen, J. W. Zhao, P. T. Ma and J. P. Wang, *Cryst. Growth Des.*, 2011, **11**, 3769; (*c*) W. L. Chen, Y. G. Li, Y. H. Wang, E. B. Wang and Z. M. Zhang, *Dalton Trans.*, 2008, 865.

14 G. M. Sheldrick, *SADABS, Program for Siemens Area Detector Absorption Corrections*: University of Göttingen, Germany, 1997.

15 (*a*) G. M. Sheldrick, *SHELXL97, Program for Crystal Structure Solution*: University of Göttingen, Germany, 1997; (*b*) G. M. Sheldrick, *SHELXL97, Program for Crystal Structure Refinement*: University of Göttingen, Germany, 1997.

16 Z. M. Zhang, Y. G. Li, S. Yao and E. B. Wang, *Dalton Trans.*, 2011, **40**, 6475.

17 U. Kortz, *J. Cluster Sci.*, 2003, **14**, 205.

18 W. L. Chen, Y. G. Li, Y. H. Wang and E. B. Wang, *Eur. J. Inorg. Chem.*, 2007, **2007**, 2216.

19 (*a*) H. H. Thorp, *Inorg. Chem.*, 1992, **31**, 1585; (*b*) I. D. Brown and D. Altermatt, *Acta Crystallogr., Sect. B: Struct. Sci.*, 1985, **41**, 244.

20 (*a*) S. Yao, J. H. Yan, H. Duan, Z. M. Zhang, Y. G. Li, X. B. Han, J. Q. Shen, H. Fu and E. B. Wang, *Eur. J. Inorg. Chem.*, 2013, **27**, 4770; (*b*) D. Y. Shi, J. W. Zhao, L. J. Chen, P. T. Ma, J. P. Wang and J. Y. Niu, *CrystEngComm*, 2012, **14**, 3108; (*c*) J. F. Cao, S. X. Liu, R. G. Cao, L. H. Xie, Y. H. Ren, C. Y. Gao and L. Xu, *Dalton Trans.*, 2008, 115.

21 R. D. Peacock and T. J. R. Weakley, *J. Chem. Soc. A*, 1971, 1937.

22 (*a*) J. Iijima and H. Naruke, *J. Mol. Struct.*, 2013, **1040**, 33; (*b*) J. Iijima, E. Ishikawa, Y. Nakamura and H. Naruke, *Inorg. Chim. Acta*, 2010, **363**, 1500.

23 (*a*) C. M. Liu, D. Q. Zhang and D. B. Zhu, *Cryst. Growth Des.*, 2005, **6**, 524; (*b*) Y. H. Liu, G. L. Guo and J. P. Wang, *J. Coord. Chem.*, 2008, **61**, 2428.

24 (*a*) X. Y. Qian, Z. Q. He, Q. Y. Wu, X. Tong, W. F. Yan and J. Gong, *Chin. Sci. Bull.*, 2011, **56**, 2327; (*b*) L. Huang, W. H. Fang, X. X. Li and G. Y. Yang, *J. Cluster Sci.*, 2011, **22**, 141.

25 (*a*) H. Y. Zhao, J. W. Zhao, B. F. Yang, H. He and G. Y. Yang, *CrystEngComm*, 2013, **15**, 5209; (*b*) H. Y. Zhao, J. W. Zhao, B. F. Yang, H. He and G. Y. Yang, *CrystEngComm*, 2013, **15**, 8186.

26 (*a*) C. Lampropoulos, T. C. Stamatatos, K. A. Abboud and G. Christou, *Inorg. Chem.*, 2008, **48**, 429; (*b*) T. Kido, Y. Ikuta, Y. Sunatsuki, Y. Ogawa, N. Matsumoto and N. Re, *Inorg. Chem.*, 2002, **42**, 398; (*c*) M. L. Kahn, C. Mathonière and O. Kahn, *Inorg. Chem.*, 1999, **38**, 3692.

27 (*a*) Z. Y. Li, G. S. Zhu, X. D. Guo, X. J. Zhao, Z. Jin and S. L. Qiu, *Inorg. Chem.*, 2007, **46**, 5174; (*b*) M. L. Kahn, C. Mathonière and O. Kahn, *Inorg. Chem.*, 1999, **38**, 3692.

